The Journal of Chemical Physics

RESEARCH ARTICLE | NOVEMBER 15 2024

Photodissociation dynamics of H_2S^+ via the $A\,^2A_1$ (0, 8, 0) state

Yuxin Tan ; Yaling Wang ; Chang Luo ; Zhiwen Luan; Jie Li; Daofu Yuan ; Xiaoguo Zhou ; Xingan Wang ; Xueming Yang

J. Chem. Phys. 161, 194301 (2024)
https://doi.org/10.1063/5.0235630

The Journal of Chemical Physics ARTICLE pubs.aip.org/aip/jcp

Photodissociation dynamics of H_2S^+ via the A^2A_1 (0, 8, 0) state

Cite as: J. Chem. Phys. 161, 194301 (2024); doi: 10.1063/5.0235630
Submitted: 28 August 2024 • Accepted: 29 October 2024 •
Published Online: 15 November 2024

Yuxin Tan,[1] Yaling Wang,[1] Chang Luo,[2] Zhiwen Luan,[1] Jie Li,[1] Daofu Yuan,[2,a)] Xiaoguo Zhou,[1] Xingan Wang,[1,3,a)] and Xueming Yang[3,4,5]

AFFILIATIONS

[1] Department of Chemical Physics, University of Science and Technology of China, Hefei 230026, China
[2] Hefei National Research Center for Physical Science at the Microscale, University of Science and Technology of China, Hefei 230026, China
[3] Hefei National Laboratory, Hefei 230088, China
[4] State Key Laboratory of Molecular Reaction Dynamics, Dalian Institute of Chemical Physics, Chinese Academy of Sciences, Dalian 116023, China
[5] Department of Chemistry, School of Science, Southern University of Science and Technology, Shenzhen 518055, China

[a)] **Authors to whom correspondence should be addressed:** ydfu@ustc.edu.cn and xawang@ustc.edu.cn

ABSTRACT

The photodissociation dynamics of the hydrogen sulfide cation (H_2S^+) (X^2B_1) were investigated using the time-sliced velocity map ion imaging technique. S^+ (^4S_u) product images were measured at four photolysis wavelengths around 393.70 nm, corresponding to the excitation of the H_2S^+ (X^2B_1) cation to the A^2A_1 (0, 8, 0) state. The raw images and the derived total kinetic energy releases (TKERs) spectra exhibited partial rotational resolution for the H_2 products. A sensitive dependence on the photolysis wavelength was observed in the TKER spectra and anisotropy parameters. Within a narrow excitation energy range of ~12 cm^{-1}, the H_2 products showed two distinct rotational excitations. Furthermore, clear differences in anisotropy parameters were observed. These phenomena indicate that the rotational excitation of the H_2S^+ ions plays a role in the non-adiabatic photodissociation dynamics.

INTRODUCTION

Hydrogen sulfide (H_2S) is a relatively abundant component in the universe.[1–4] It has attracted significant attention in both interstellar observations[1–4] and combustion processes.[5,6] Molecular ions formed through various processes play an important role in the chemical evolution of interstellar clouds due to their high reactivity.[7–9] Investigating the H_2S^+ cation is therefore essential for understanding astrochemical networks involving sulfur species. Photochemical studies on H_2S have also greatly enhanced our understanding of the sulfur cycle. In addition, the H_2S^+ cation serves as an ideal model for studying non-adiabatic interactions.[10–12]

The rovibronic transition structures of the H_2S^+ cation have attracted sustained research interest. The H_2S^+ cation, in its ground electronic state X^2B_1, has a bent equilibrium molecular structure, similar to the H_2S molecule. Nevertheless, the first excited state A^2A_1 of the H_2S^+ cation has a larger HSH angle in equilibrium configuration, compared to the X^2B_1 state. Interestingly, the X^2B_1 and A^2A_1 states degenerate to a $^2\Pi_u$ state at a linear configuration, resulting in strong Renner–Teller couplings between the two states above the linear barrier.[11,13] The vibronic structures of H_2S^+ were investigated using various experimental techniques, such as photoelectron spectroscopy,[14–16] photoionization,[17] mass spectroscopy,[18,19] optical emission spectroscopy,[10,14] and photoelectron–photoion coincidence measurements.[20] Horani *et al.* observed the first emission spectrum of H_2S^+ cations within the 400–600 nm range.[21] However, the confirmation of the spectrum assignment was delayed until the availability of photoelectron spectroscopy data for H_2S.[14] In 1971, Dixon *et al.* carried out a photoelectron spectroscopic study on H_2S and performed a comparison with the corresponding emission spectrum of H_2S^+.[14] Their results showed prominent vibronic structures attributed to the bending excitation of the upper

A^2A_1 state of the H_2S^+ cation, resulting from the significant change in the equilibrium configuration of the H_2S^+ A^2A_1 state.[14] In 1995, Baltzer *et al.* performed a high-resolution photoelectron spectroscopic study on H_2S and observed detailed vibronic structures with different K values attributed to the X^2B_1 and A^2A_1 states of the H_2S^+ cation.[15] In 2004, Hochlaf *et al.* performed a photoelectron spectroscopic study of H_2S with improved spectral resolution and observed weak combinational transitions of the symmetric stretching mode (ν_1) and bending mode (ν_2).[16] In 2010, Han *et al.* employed mass analyzed threshold ionization (MATI) combined with the photo-fragment excitation technique to assign the rotationally resolved transition bands of H_2S^+ above the linear barrier.[19] The spectroscopic studies mentioned earlier provided us with a comprehensive understanding of the transitions between the lowest X^2B_1, A^2A_1, and B^2B_2 states of the H_2S^+ cation.

The dissociation of the H_2S^+ cation via the A^2A_1 state has also continued to draw significant experimental interest. In 1968, Dibeler and Liston conducted a combined vacuum-ultraviolet (VUV) mass spectrometric study of H_2S photoionization and determined the energy threshold associated with the $H_2S^+ \rightarrow S^+ + H_2$ process.[17] Dixon *et al.* further proposed that the H_2S^+ cations at the A^2A_1 state can predissociate within the interaction of the X^2B_1 state and the repulsive $^4A_2$ state.[14] They noticed that the $0\text{–}\nu_2'$ bands with $\nu_2' \geq 8$ were missing in the emission spectrum compared to the photoelectron results with similar Franck–Condon excitations, suggesting the occurrence of predissociation at high vibrational levels.[14] In 1975, Möhlmann and Deheer measured the lifetimes of excited H_2S^+ cations at the A^2A_1 state by measuring the decay curves of the $A^2A_1 \rightarrow X^2B_2$ emission bands of the H_2S^+ cation.[22] Their results indicated the existence of the decay channel.[22] In 1979, Eland measured the time-of-flight (TOF) spectra from H_2S^+ dissociation and observed the $S^+ + H_2$ and $SH^+ + H$ channels.[20] In 2007, Webb *et al.* employed the time-sliced velocity map ion imaging (VMI) technique to study the photodissociation dynamics of H_2S^+ cations in the 300–420 nm region involving the one photon $A^2A_1 \leftarrow X^2B_1$ excitation of the H_2S^+ cation.[23,24] They observed the nuclear-spin correlated behavior tracing back to the parent H_2S^+ cations and confirmed two possible dissociation pathways for the A^2A_1 state, which evolve toward X^2B_1 and B^2B_2 states via different interactions (referred to as pathway I and pathway II) and ultimately dissociate via the repulsive $^4A_2$ state within the spin–orbit coupling interaction.[23,24]

Numerous theoretical efforts have also been devoted to studying this non-adiabatic system using various theoretical methods, providing significant insights into the molecular structures, potential energy surfaces (PESs), and dynamic behaviors of the H_2S^+ cation.[11,13,25–30] During these works, the effects of symmetries (C_{2v} and C_s) have been carefully considered. Through analysis of the calculated PESs, a deeper and more comprehensive understanding of the observed experimental results has been achieved.

Recently, researchers have observed competitive non-adiabatic photodissociation dynamics of H_2S^+ near 337 nm.[30] Two possible nonadiabatic pathways were revealed through analyzing the characterization of the constructed global full-dimensional PESs.[30] The calculated PES results (as shown in Fig. 3 of Ref. 30) show the existence of a first-order saddle point (TS1) connecting two minima (M1 and M2), located on the A^2A_1 PES. The experimental and theoretical results indicate that the TS1 plays a role in the non-adiabatic photodissociation dynamics [see Fig. 4(a) of Ref. 30 for the minimum energy path]. The first dissociation pathway (pathway I) proceeds via Renner–Teller coupling or spin–orbit coupling toward the X^2B_1 state, as confirmed in previous studies, with the HSH angle increasing and decreasing during dissociation when the excitation energy is not enough to overcome the TS1. On the contrary, another pathway occurs when the excitation is sufficient to overcome the TS1, allowing the H_2S^+ cations evolving on the A^2A_1 PES toward the continual approaching of two H atoms, accessing products via spin–orbit coupling to the $^4A_2$ state. This pathway differs from pathways I and II, as confirmed by Ashfold *et al.*, and is referred to as pathway III here. The subsequent study near 325 nm confirmed that dissociation pathway II involves vibronic coupling with the $^2B_2$ state in the conical intersection region, followed by spin–orbit coupling to the $^4A_2$ state, and ultimately dissociating into H_2 ($X^1\Sigma_g^+$) + S^+ (^4S_u) products.[31]

In this study, we present a high-resolution experimental study on the H_2S^+ photodissociation via the excitation to the A^2A_1 (0, 8, 0) state that could shed new insights into the photodissociation dynamics. The current excitation energy of ~25 406 cm^{-1} was slightly above the linear barrier of H_2S^+ (X^2B_1 and A^2A_1 states)[16] by about 2200 cm^{-1}. Compared to previous studies,[30–32] this work further extends the investigation of the photodissociation dynamics of H_2S^+ with relatively lower bending vibration excitation. The H_2S^+ X^2B_1 cations, produced via a (2 + 1) REMPI strategy, were excited to the A^2A_1 (0, 8, 0) $K = 1$ state via one-photon absorption near 393.70 nm. The S^+ products were probed by the time-sliced VMI technique, allowing the simultaneous detection of product energy and angular distributions with high resolution. The derived product total kinetic energy release spectra and the anisotropy parameters exhibited a sensitive dependence on the excitation wavelengths, which was attributed to the various transitions of A^2A_1 (0, 8, 0) $\leftarrow X^2B_1$ (0, 0, 0) via different initial rotational states of H_2S^+ X^2B_1. The results indicated the effect of the rotational excitation of H_2S^+ on the photodissociation dynamics, resulting in significant variations in product energy and angular distributions.

EXPERIMENTAL METHOD

The experimental setup is schematically depicted and detailed in previous publications.[30–32] A 1600 l/s turbomolecular pump was used to pump the source chamber, reaching a baseline pressure of 9×10^{-9} Torr. Meanwhile, another turbomolecular pump (700 l/s) was used to evacuate the detection chamber, with a background pressure of 5×10^{-8} Torr. These pressures were recorded without molecular beam injection. A pulsed valve (Parker Series 9, 1 mm nozzle diameter) was utilized to generate an H_2S beam (T_{rot} = ~30 K) via supersonic expansion. Argon, containing 10% H_2S, served as the carrier gas, maintaining a working pressure of 2 bars. The produced H_2S beam was successively collimated using the skimmer and the first repeller plate of the ion optics (with a central aperture) on the propagation axis. The aperture diameters for the skimmer and the plate were both 2 mm. H_2S^+ cations in the X^2B_1 (0, 0, 0) state were generated via the (2 + 1) REMPI process of H_2S, which excited H_2S molecules from their electronically ground state to the $^1A_1(\ldots 2b_1{}^1 4pb_1{}^1)$ Rydberg intermediated state followed by one photon ionization.[23,24,30] The rotational distribution of H_2S^+ is different from that of H_2S (more details in the supplementary material).

The tunable photolysis laser, propagating in the counter direction, activated the dissociation process. The H_2S^+ cations were one-photon excited via the A^2A_1 (0, 8, 0) $K = 1 \leftarrow X^2B_1$ (0, 0, 0) transition, followed by dissociation into H_2 ($X^1\Sigma_g^+$) + S^+ (^4S_u) products. Circular polarization was applied to the ionization laser to dismiss polarization effects. A lower pulse energy was applied to the ionization laser beam to limit the Coulomb interactions of parent H_2S^+ cations. The photolysis laser was tunable near 393.70 nm, keeping the polarization direction parallel to the detector plane. The photolysis laser was focused using a 300 mm lens, the same as that used for the ionization laser. The laser beams overlapped spatially, with a 40 ns time delay between them. The S^+ products, forming in the ^4S_u state, reached and impacted the particle detector after being accelerated by the ion optics. The expanded S^+ ion spheres were mass-selected and time-sliced via a rapid high-voltage pulse (~30 ns duration). The raw images of S^+ ions in the detector were recorded and stored using a CCD camera and a computer workstation.

RESULTS AND DISCUSSION

Experimental ion images

The images of S^+ (^4S_u) were measured at four different photolysis wavelengths: 393.59, 393.68, 393.70, and 393.77 nm. The photolysis wavelengths correspond to the resonance peaks of the photofragment excitation (PHOFEX) spectra via the A^2A_1 (0, 8, 0) $K = 1$ state, as shown in Fig. S1 of the supplementary material. The PHOFEX spectrum was measured by acquiring the S^+ product signal as a function of the tunable photolysis laser wavelength around 393.70 nm, while the photoionization laser was fixed at 302.6 nm. Figure 1 presents the recorded raw images of S^+ (^4S_u), marking the photolysis laser polarization with a red arrow. Background signals of S^+ (^4S_u), primarily arising from the focused ionization laser, were accumulated with the photolysis laser turned off and subsequently subtracted from the images obtained with the photolysis laser active. Throughout the experimental procedure, the signal-to-noise ratio consistently exceeded 20, as determined by counting the total S^+ events within the kinetic energy range of the excitation photon.

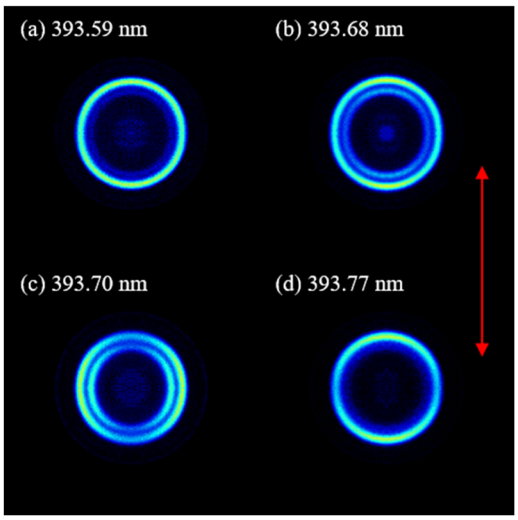

FIG. 1. Ion images of S^+ (^4S_u) from the photodissociation of H_2S^+ (X^2B_1) at (a) 393.59 nm, (b) 393.68 nm, (c) 393.70 nm, and (d) 393.77 nm. The polarization direction of the photolysis laser is represented schematically by a vertical double-headed arrow. The observed rings correspond to the H_2 ($v = 0$, j) products.

The H_2 ($X^1\Sigma_g^+$, $v = 0$) products in different rotational states exhibited various velocities, underlined in the concentric rings in Fig. 1. The intensity variations indicate distinct dynamic behaviors for each photolysis wavelength, such as branching ratios and angular distributions. At 393.68 and 393.70 nm, the images presented dual ring structures with high resolution.

Product total kinetic energy releases

The total kinetic energy release (TKER) spectra were converted from the S^+ images in Fig. 1 and illustrated in Fig. 2. In each panel, the results of a multi-peak fitting of the TKER spectra are represented by a red solid line, with the rotational states indicated by a series of green lines. The branching ratios of the rotational states were derived through the spectrum fitting. The TKER associated with the photodissociation process is quantified by the following equation:

$$\mathrm{TKER} = E_{\mathrm{int}}(H_2S^+) + E_{h\nu} - D_0(S^+ - H_2) - E_{\mathrm{int}}(H_2) - E_{\mathrm{int}}(S^+), \quad (1)$$

where $E_{\mathrm{int}}(H_2S^+)$ denotes the initial internal energy of H_2S^+, which will be discussed later. $E_{h\nu}$ represents the photon energy for the excitation of H_2S^+ in the X^2B_1 state, and $D_0(S^+–H_2)$ denotes the bond dissociation energy for the formation of S^+ (^4S_u) and H_2 ($X^1\Sigma_g^+$, $v = 0$, $j = 0$) pair-products, as confirmed by previous studies.[16,24] Under the energy limitation of one-photon excitation, the only product channel yields S^+ in its electronically ground state and recoiled H_2 products with rovibrational excitations. Therefore, the internal energy term for S^+ is assumed to be zero and denoted as $E_{\mathrm{int}}(S^+)$. As the available energy is not sufficient for the vibrational excitation of H_2, only rotational excitation is considered to calculate the $E_{\mathrm{int}}(H_2)$ term.

Consistent with the two-ring structures observed in the images at the wavelengths of 393.68 and 393.70 nm, the derived TKER spectra displayed clear bimodal features near 1500 and 1000 cm^{-1}, as shown in Fig. 2. According to the energy comb displayed at the top of each TKER spectrum, the main peak, which corresponds to the partially resolved outermost ring, can be attributed to the H_2 ($X^1\Sigma_g^+$, $v = 0$, $j = 0$–2) products. In addition, the well-resolved secondary peak also corresponds to the H_2 ($X^1\Sigma_g^+$, $v = 0$, $j = 3$) products. However, the bimodal peak structure of the TKER spectra vanished at the wavelengths of 393.59 and 393.77 nm. The secondary peak near 1000 cm^{-1} diminishes to show a shoulder structure, indicating that nearly all available energy was transferred into the translational motions of the products. It is worth noting that the remarkably different features in the TKER spectrum suggest that the S^+ (^4S_u) products are likely formed via different initial states (*vide infra*). In particular, the separation of the resolved primary peak and secondary peak (shoulder peak) is about 587 cm^{-1}, which matches nicely with the energy difference between H_2 ($v = 0$, $j = 1$) and H_2 ($v = 0$, $j = 3$) states. Comparing the alignment of the resolved peaks with the energy combs calculated under the

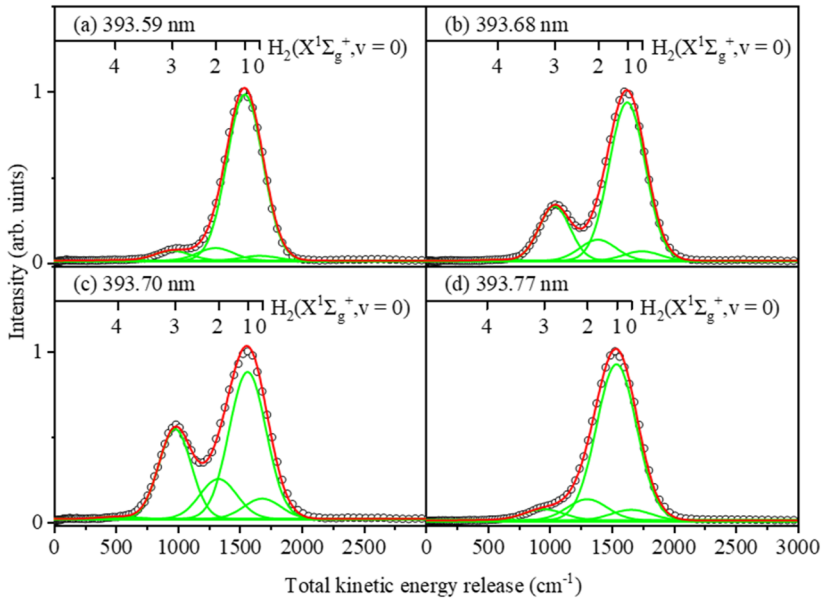

FIG. 2. Total kinetic energy release (TKER) distributions from photolysis of H_2S^+ (X^2B_1) at (a) 393.59 nm, (b) 393.68 nm, (c) 393.70 nm, and (d) 393.77 nm. The calculated energy combs indicating the j states of H_2 ($X^1\Sigma_g^+$, $v = 0$) are shown at the top of each spectrum. The energy combs were calculated by taking the $E_{int}(H_2S^+)$ term into account, as discussed in the main text.

$E_{int}(H_2S^+) = 0$ assumption, the rotational peaks in the TKER spectrum of the product shifted by 20, 110, 50, and 30 cm^{-1} toward higher translational kinetic energies at the photolysis wavelengths of 393.59, 393.68, 393.70, and 393.77 nm, respectively. A similar phenomenon, where higher rotational distributions than the available energy were observed, was also noted by Zanganeh *et al.* in their study of the product fluorescence signal of H_2O photodissociation.[33,34] It indicates that the initial rotational excitation of the parent H_2S^+ cation in the X^2B_1 (0, 0, 0) state cannot be ignored. The rotational temperature of H_2S was about 30 K. The ionization of H_2S was achieved by the (2 + 1) REMPI process, which would further change the rotational states and produce a different rotational distribution for H_2S^+ compared to the H_2S beam.[23] Subsequently, the rotationally excited H_2S^+ cations in the X^2B_1 (0, 0, 0) state were selectively excited using the photolysis laser at certain wavelengths and followed by photodissociation, leading to energy shifts between the observed TKER spectra and the combs calculated by assuming $E_{int}(H_2S^+) = 0$. Hence, the energy shifts mentioned earlier were considered the internal energy terms of H_2S^+ and introduced into Eq. (1) to derive the corrected energy combs. Involving consideration of the internal energy of H_2S^+ in the X^2B_1 (0, 0, 0) state, the fitting of the TKER spectra was performed. The fitting results are displayed in Fig. 2 with the corrected energy combs.

Product angular distributions

The product angular distribution for a photodissociation process induced by one-photon excitation can be mathematically described as a function of the recoil velocity angle relative to the photolysis laser polarization,

$$I(\theta) \propto (1/4\pi)(1 + \beta P_2(\cos\theta)). \tag{2}$$

In this expression, the recoil velocity angle is denoted as θ, and the second Legendre polynomial $P_2(\cos\theta)$ is used. The anisotropy parameter, β, characterized the derived image angular distribution within a [−1, 2] range. Typically, β, which correlates with individual rotational states of H_2, was calculated by mathematical fitting employing the formula of Eq. (2). Figure 3 illustrates the β values for all available H_2 ($v = 0$, j) states, within the excitation energy limitation. In addition, the mean β values at four different wavelengths are calculated to be 0.12, 0.27, −0.37, and 0.46, respectively, by fitting the signal angular distributions over the whole kinetic range. The results show that the product angular distributions strongly depend on the photolysis wavelength. At 393.59 nm, the averaged β value is close to 0, indicating an isotropic angular distribution of the products. This suggests that the dissociation process is slower than at other photolysis wavelengths, allowing enough time for the ions to rotate and resulting in a smeared-out angular distribution. At 393.68 and 393.77 nm, the corresponding average β values of

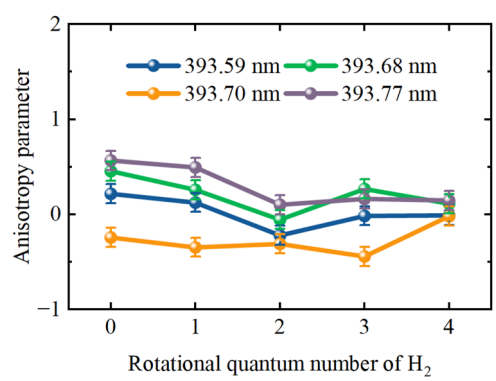

FIG. 3. Anisotropy parameters for various rotational states of H_2 ($X^1\Sigma_g^+$, $v = 0$) products at four different photolysis wavelengths. The uncertainty of the β values is estimated to be ±0.1.

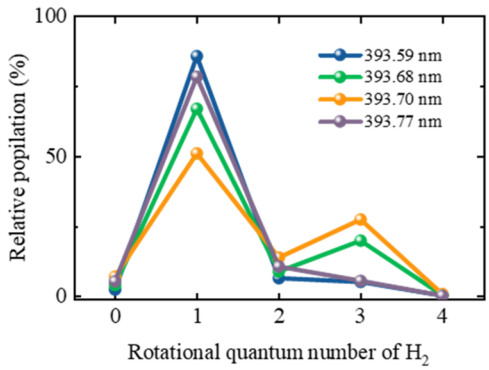

FIG. 4. Branching ratios of rotational states for H_2 ($X^1\Sigma_g^+$, v = 0) products resulting from the S^+ ($^4S_u^+$) + H_2 ($X^1\Sigma_g^+$) channel.

0.27 and 0.46, respectively, indicate a parallel photodissociation process. Meanwhile, at 393.70 nm, the averaged β value of −0.37 indicates a process dominated by a perpendicular transition. The β values for the j = 0–4 rotational states vary around the averaged β value at the four photolysis wavelengths.

Product branching ratios

Figure 4 presents the branching ratios of various rotational states of H_2 ($X^1\Sigma_g^+$, v = 0) derived from the multi-peak fitting of the TKER spectra. The results indicate that more than 50% of the internal energy of H_2 products is distributed in the H_2 (v = 0, j = 1) state across all four photolysis wavelengths. In particular, the rotational branching ratios for H_2 ($X^1\Sigma_g^+$, v = 0, j = 1) are 86%, 67%, 51%, and 78% at 393.59, 393.68, 393.70, and 393.77 nm, respectively. Notably, at 393.68 and 393.70 nm, the rotational branching ratios for H_2 ($X^1\Sigma_g^+$, v = 0, j = 3) are 20% and 27%, respectively, indicating that the internal energy of H_2 ($X^1\Sigma_g^+$, v = 0) is significantly higher at these wavelengths compared to the other two.

Photodissociation dynamics

Previous studies have proposed three plausible mechanisms for the dissociation of H_2S^+ (A^2A_1) into H_2 ($X^1\Sigma_g^+$) + S^+ (^4S_u). Dixon first suggested a mechanism involving Renner–Teller coupling to the X^2B_1 state at a near-linear configuration, followed by spin–orbit coupling to the repulsive $^4A_2$ state at smaller bond angles.[14] Hirst proposed an alternative route involving vibronically facilitated nonadiabatic transfer from the A^2A_1 state to the B^2B_2 state, followed by spin–orbit coupling to the $^4A_2$ state.[27] Webb *et al.* discovered that the first mechanism involving Renner–Teller coupling yields rotationally and vibrationally cold H_2 products.[23] In contrast, the latter mechanism has a higher excitation threshold (~335 nm), producing H_2 products with higher vibrational and rotational excitation.[23] Recently, a third mechanism has been proposed by Luan *et al.* They found the dissociation pathway involving the direct spin–orbit coupling between A^2A_1 and $^4A_2$ states, crossing the TS1 on the A^2A_1 state.[31] In the current work, the photolysis laser was set to around 393.70 nm, which is about 2200 cm^{-1} above the linear barrier of H_2S^+ cations. Given this excitation energy, H_2S^+ cations are not sufficiently energetic to reach the conical intersection region proceeding via the second pathway or to overcome the TS1 undergoing the third pathway. Hence, the first mechanism appears to be the major contribution in our study. H_2S^+ cations in the X^2B_1 (0, 0, 0) state were initially excited to the A^2A_1 (0, 8, 0) K = 1 state, followed by Renner–Teller coupling to the X^2B_1 state with high bending vibrational excitation, and subsequently by spin–orbit coupling to the repulsive $^4A_2$ state, which adiabatically correlates with the H_2 ($X^1\Sigma_g^+$) + S^+ (^4S_u) product channel. In addition, the nonadiabatic transition of the H_2S^+ from the A^2A_1 state to the X^2B_1 state can also be facilitated via spin–orbit coupling.[31]

However, the observed dependence of the product state distribution and angular distribution, within a narrow excitation energy range of ~12 cm^{-1}, cannot be fully accounted for by the electronic state evolution pathways of H_2S^+ cations. The experimental results at photolysis wavelengths of 393.59 and 393.77 nm show that the co-fragments H_2 ($X^1\Sigma_g^+$, v = 0) are rotationally "cold," as evidenced by the single product ring observed in the images. At 393.68 and 393.70 nm, the H_2 products exhibit higher rotational excitation. Previous studies have indicated that the dissociation of the A^2A_1 state via the Renner–Teller coupling with the X^2B_1 state under the C_{2v} symmetry produces H_2 with cold rotational excitation.[23,31] Hanazaki investigated the influence of parent rotation on product rotation by separating parent rotation from other factors affecting product rotational excitation.[35] Although this approach may overestimate the effect, Hanazaki suggested that parent rotation can, in some cases, substantially influence product rotation.[35] In 2010, Han *et al.* investigated the spectroscopy of the $A^2A_1 \leftarrow X^2B_1$ transition of H_2S^+ ions using the MATI-PHOFEX technique.[19] They measured rotationally resolved PHOFEX spectra corresponding to the highly excited states of H_2S^+ (A^2A_1, ν_2 = 7, 8, 9) with different K quantum numbers above the linear barrier. Based on their peak assignment in high-resolution spectra, the four photolysis wavelengths studied in this work correspond to the A^2A_1 (0, 8, 0) K = 1 ← X^2B_1 transition of H_2S^+. In addition, the presence of spin–orbit splitting introduces complexity to the transition spectra within the investigated energy range. This suggests that the excitation process at the four studied photolysis wavelengths involves multiple rotational transitions. The two distinct patterns observed in the TKER spectra—one characterized by cold rotational excitation of H_2 products at 393.59 and 393.77 nm, and the other characterized by the higher rotational excitation of H_2 products at 393.68 and 393.70 nm—highlight the significant effects of the rotational excitation on the nonadiabatic coupling between the X^2B_1 and A^2A_1 states.[36–38]

The H_2S^+ preparation was achieved by the (2 + 1) REMPI scheme via the $^1A_1 \leftarrow X^1A_1$ transition of H_2S in this work. The H_2S molecules were initially two-photon resonantly excited to the $^1A_1$ Rydberg state, followed by the ionization of a $4pb_1$ electron of the $^1A_1$ Rydberg state by the third photon. The (2 + 1) REMPI process can yield different rotational distributions for H_2S^+ compared to H_2S.[23] More details of the rotational excitation analysis of H_2S^+ are given in the supplementary material. It is challenging to achieve accurate rotational assignments for the prepared H_2S^+ and the excitation transitions of H_2S^+ at the four studied photolysis wavelengths.[19] A qualitative estimation of the rotational excitation of H_2S^+ can be reached. The rotational constants A, B, and C of H_2S^+ at the ground vibronic states are 10.17, 8.59, and 4.57 cm^{-1}, respectively. Then, the energies of the rotational states, such as

J_{KaKc} = 3_{13}, 3_{30}, 4_{04}, and 4_{14}, are estimated to be around 110 cm^{-1}. In other words, a rotational energy around 110 cm^{-1} can be reached by a moderate J quantum number of H_2S^+ in the X^2B_1 state. It suggests that the observed shifts in the TKER spectra are attributed to the rotational excitation of the prepared H_2S^+ X^2B_1 (0, 0, 0) state via the (2 + 1) REMPI process. This is consistent with the analysis according to the photoelectron spectrum of H_2S measured in the (2 + 1) REMPI process, as seen in the supplementary material.

The H_2S^+ ion is an asymmetric molecular cation. The molecular axes of H_2S^+ are defined as follows: the a-axis is parallel to the H–H bond, the b-axis is parallel to the C_{2v} axis, and the c-axis is perpendicular to the H–S–H^+ molecular plane. Along the dissociation coordinate, the excited H_2S^+ ion in the A^2A_1 state is non-adiabatically coupled to the X^2B_1 state and consequently coupled to the repulsive 1^4A_2 state with large S^+–H_2 separations. The rotation about the b-axis is likely to promote the rotational excitation of the H_2 product, while the rotations about the a-axis and the c-axis are more likely portioned into product orbital angular momentum, as suggested by Jarrold *et al.*[18] and Webb *et al.*[23] In other words, the rotation about the b-axis of H_2S^+ could have a role in the rotational excitation of the H_2 product. In this work, the H_2S^+ cations were excited to different rotational levels in the A^2A_1 state at four specific photolysis wavelengths: 393.59, 393.68, 393.70, and 393.77 nm. The observed two patterns of the H_2 rotational excitation may result from the different rotational excitations about the b-axis (C_2 axis in C_{2v}) of the excited H_2S^+ in the A^2A_1 state.

There is also a great wealth of underlying dynamics in the observed product angular distribution. The initial $A^2A_1 \leftarrow X^2B_1$ transition should be perpendicular to the H–S–H^+ plane and along the c axis, similar to the $A^2A'' \leftarrow X^2A'$ transition of the HCO.[39] Negative β values would be expected for a direct dissociation process. However, the product anisotropy parameters vary significantly depending on the photolysis photon energy. In particular, at 393.68 and 393.70 nm, the small difference in excitation energy (less than 2 cm^{-1}) leads to substantial variations in anisotropy parameters (see Fig. 3). For $H_2(j = 1–3)$ products, the β values are between −0.5 and 0 at 393.70 nm, while the β values are between 0.5 and 0 at 393.68 nm. At 393.59 and 393.77 nm, the β values are mostly positive. A similar phenomenon, parallel product recoil distributions from the perpendicular initial transition, has also been observed in the HCO photodissociation by Kable *et al.*[39] They suggested that (1) the transient exchange of angular momentum between electrons and nuclei and (2) the rotation about the top axis provide a reasonable explanation to the observed positive β values. Since the H_2S^+ was resonantly excited from the rotational levels of the X^2B_1 state, the excited H_2S^+ in the upper A^2A_1 state can have non-zero $\langle J_a^2 \rangle$ values. The a-axis rotation transforming as b_1 (in C_{2v} symmetry) can facilitate the non-adiabatic coupling of the $^2A_1$ state to a $^2B_1$ symmetry. The Coriolis coupling resulting from the rotational excitation about the a-axis could lead to a force perpendicular to the H–S–H^+ plane, consistent with expected positive β values. A similar rotational state-dependent effect on molecular photodissociation dynamics has also been discovered in photodissociation studies of H_2O and H_2S.[2,40–42] The electronic Coriolis coupling arising from $\langle J_a^2 \rangle$ in the $C^1B_1 \rightarrow B^1A_1$ transition of H_2O molecules leads to a distinct OH(X) product distribution (preferentially parallel to the polarization vector of the photolysis laser ε_{phot}) compared with the homogeneous dissociation pathway.[36,37] In the photodissociation of $H_2S(^1B_1)$, the $S(^1D)$ + H_2 channel dissociating via the Coriolis-induced mechanism also exhibits distinct product distribution (preferentially parallel to the polarization vector of photolysis laser ε_{phot}) compared with the homogeneous dissociation mechanism.[2] It is indicated that the non-zero $\langle J_b^2 \rangle$ component promotes the non-adiabatic transition of H_2S from $^1B_1$ to a $^1B_2$ symmetry.[2] The observed variation in product angular distribution highlights the effect of the a-axis rotation of H_2S^+.

CONCLUSIONS

In summary, the photodissociation dynamics of H_2S^+ (X^2B_1) via one-photon excitation to the A^2A_1 (0, 8, 0) K = 1 state has been studied near 393.70 nm using the VMI technique. The dissociation pathway in this study is consistent with the interaction involving A^2A_1, X^2B_1, and $^4A_2$ states. The H_2S^+ cations undergo one-photon excitation from the X^2B_1 (0, 0, 0) state to high vibrational states on the A^2A_1 PES. This is followed by Renner–Teller coupling (or spin–orbit coupling) back to highly vibrationally excited states of X^2B_1 and ultimately coupling to the $^4A_2$ state via spin–orbit interaction. A sensitive wavelength dependence is observed for the product angular distributions and rotational branching ratios. Two distinct rotational distributions of H_2 products are observed in the spectra at four photolysis wavelengths. It indicates that the rotational excitation about the b-axis (C_2 axis in C_{2v}) of the excited H_2S^+ can influence the rotational distribution of H_2 products during the non-adiabatic dissociation process. The observed variations in anisotropy parameters further underscore the complexity of the dissociation process within such a small excitation energy range. It suggests that the Coriolis coupling arising from non-zero $\langle J_a^2 \rangle$ components plays a role in the dissociation process. This work presents a qualitative explanation of H_2S^+ photodissociation dynamics near the linear barrier, offering a comprehensive set of high-resolution experimental results on the rich photodissociation dynamics of H_2S^+ over a range of photolysis energies. Further accurate theoretical calculations are needed to elucidate the underlying effects in this complex nonadiabatic system.

SUPPLEMENTARY MATERIAL

See the supplementary material for the photofragment excitation (PHOFEX) spectrum of H_2S^+ (Fig. S1), the photoelectron spectrum for the $H_2S^+ \leftarrow H_2S$, $X^2B_1 \leftarrow X^1A_1$ ionization (Fig. S2), and the rotational excitation analysis of H_2S^+.

ACKNOWLEDGMENTS

This work was supported by the National Natural Science Foundation of China (Grant Nos. 22125302 and 22327801), the Innovation Program for Quantum Science and Technology (Grant No. 2021ZD0303304), and the University of Science and Technology of China. We acknowledge Baokun Shan, Ning Zhang, and Xinlang Yang for their help during the experiments.

AUTHOR DECLARATIONS

Conflict of Interest

The authors have no conflicts to disclose.

Author Contributions

Y.T. and Y.W. contributed equally to this work.

Yuxin Tan: Data curation (lead); Formal analysis (lead); Investigation (lead); Methodology (equal); Validation (lead); Writing – original draft (lead); Writing – review & editing (equal). **Yaling Wang**: Data curation (equal); Investigation (equal); Methodology (equal). **Chang Luo**: Formal analysis (supporting); Methodology (equal). **Zhiwen Luan**: Investigation (equal); Methodology (equal). **Jie Li**: Investigation (equal); Methodology (equal). **Daofu Yuan**: Supervision (equal); Writing – review & editing (lead). **Xiaoguo Zhou**: Methodology (supporting). **Xingan Wang**: Conceptualization (lead); Funding acquisition (lead); Project administration (lead); Resources (lead); Supervision (lead); Writing – review & editing (lead). **Xueming Yang**: Conceptualization (equal); Supervision (equal).

DATA AVAILABILITY

The data that support the findings of this study are available from the corresponding authors upon reasonable request.

REFERENCES

[1] J. M. Zhou, Y. R. Zhao, C. S. Hansen, J. Y. Yang, Y. Chang, Y. Yu, G. K. Cheng, Z. C. Chen, Z. G. He, S. R. Yu, H. B. Ding, W. Q. Zhang, G. R. Wu, D. X. Dai, C. M. Western, M. N. R. Ashfold, K. J. Yuan, and X. M. Yang, "Ultraviolet photolysis of H_2S and its implications for SH radical production in the interstellar medium," Nat. Commun. **11**(1), 1547 (2020).

[2] Y. R. Zhao, Z. J. Luo, Y. Chang, Y. C. Wu, S. E. Zhang, Z. X. Li, H. B. Ding, G. R. Wu, J. S. Campbell, C. S. Hansen, S. W. Crane, C. M. Western, M. N. R. Ashfold, K. J. Yuan, and X. M. Yang, "Rotational and nuclear-spin level dependent photodissociation dynamics of H_2S," Nat. Commun. **12**(1), 4459 (2021).

[3] T. H. G. Vidal, J. C. Loison, A. Y. Jaziri, M. Ruaud, P. Gratier, and V. Wakelam, "On the reservoir of sulphur in dark clouds: Chemistry and elemental abundance reconciled," Mon. Not. R. Astron. Soc. **469**(1), 435–447 (2017).

[4] Y. Oba, T. Tomaru, T. Lamberts, A. Kouchi, and N. Watanabe, "An infrared measurement of chemical desorption from interstellar ice analogues," Nat. Astron. **2**(3), 228–232 (2018).

[5] S. L. Guo, F. Zhou, J. J. Shan, Y. Y. Wang, W. Zeng, Y. F. Gao, L. Ding, and F. C. Wang, "Comparison of three combustion modes of H_2S-CO_2 gas in Claus furnace for promoting reaction temperature," Fuel **367**, 131242 (2024).

[6] A. Raj, S. Ibrahim, and A. Jagannath, "Combustion kinetics of H_2S and other sulfurous species with relevance to industrial processes," Prog. Energy Combust. Sci. **80**, 100848 (2020).

[7] B. A. McGuire, O. Asvany, S. Brunken, and S. Schlemmer, "Laboratory spectroscopy techniques to enable observations of interstellar ion chemistry," Nat. Rev. Phys. **2**(8), 402–410 (2020).

[8] M. Deiß, S. Willitsch, and J. Hecker Denschlag, "Cold trapped molecular ions and hybrid platforms for ions and neutral particles," Nat. Phys. **20**(5), 713–721 (2024).

[9] X. Jiang, L. N. Wang, G. Rauhut, X. L. Li, J. L. Hong, M. F. Zhou, and X. Q. Zeng, "Spectroscopic characterization and photochemistry of HC_3N^- and $CH_3C_3N^-$: Implications for ion chemistry in Titan's atmosphere," Mon. Not. R. Astron. Soc. **527**(3), 8996–9003 (2024).

[10] G. Duxbury, J. Rostas, and M. Horani, "Rotational analysis of the electronic emission spectrum of the H_2S^+ ion radical," Proc. R. Soc. A **331**(1584), 109–137 (1972).

[11] P. J. Bruna, G. Hirsch, M. Peric, S. D. Peyerimhoff, and R. J. Buenker, "A theoretical study of the lowest $^2B_1$, $^2A_1$ and $^2B_2$ electronic states in H_2S^+ and a comparison with corresponding states in related systems," Mol. Phys. **40**(3), 521–537 (1980).

[12] G. Duxbury, C. Jungen, A. Alijah, J. P. Maier, and D. Klapstein, "The Renner–Teller effect observed in the and electronic states of H_2S^+," Mol. Phys. **112**(23), 3072–3084 (2014).

[13] D. M. Hirst, "*Ab initio* potential-energy surfaces for the $\tilde{X}\ ^2B_1$, $\tilde{A}\ ^2A_1$, and $\tilde{B}\ ^2B_2$ states of the H_2S^+ molecular ion," J. Chem. Phys. **118**(20), 9175–9184 (2003).

[14] R. N. Dixon, G. Duxbury, M. Horani, and J. Rostas, "The H_2S^+ radical ion. A comparison of photoelectron and optical spectroscopy," Mol. Phys. **22**(6), 977–992 (1971).

[15] P. Baltzer, L. Karlsson, M. Lundqvist, B. Wannberg, D. M. P. Holland, and M. A. Macdonald, "An experimental study of the valence shell photoelectron spectrum of hydrogen sulphide," Chem. Phys. **195**(1-3), 403–422 (1995).

[16] M. Hochlaf, K. M. Weitzel, and C. Y. Ng, "Vacuum ultraviolet pulsed-field ionization-photoelectron study of H_2S in the energy range of 10–17 eV," J. Chem. Phys. **120**(15), 6944–6956 (2004).

[17] V. H. Dibeler and S. K. Liston, "Mass-spectrometric study of photoionization. XI. Hydrogen sulfide and sulfur dioxide," J. Chem. Phys. **49**(2), 482–485 (1968).

[18] M. F. Jarrold, A. J. Illies, and M. T. Bowers, "Mechanism of the metastable reaction $H_2S^+ \rightarrow S^+ + H_2$; product energy distributions and their dependence on temperature," Chem. Phys. **65**(1), 19–28 (1982).

[19] S. Han, T. Y. Kang, and S. K. Kim, "Rotationally resolved spectroscopy of the $\tilde{A}\ ^2A_1 \leftarrow \tilde{X}\ ^2B_1$ transition of H_2S^+ above the barrier to linearity using the mass-analyzed threshold ionization photofragment excitation technique," J. Chem. Phys. **132**(12), 124304 (2010).

[20] J. H. D. Eland, "Dissociations of state-selected $C_2H_2^+$ and D_2S^+ studied by photoelectron-photoion coincidence spectroscopy," Int. J. Mass Spectrom. Ion Phys. **31**(1–2), 161–173 (1979).

[21] M. Horani, S. Leach, and J. Rostas, *VIe Conférence Internationale sur les phénomènes d'ionisation dans les gaz* (SERMA, 1963), Vol. I, p. 45.

[22] G. R. Möhlmann and F. J. Deheer, "Lifetimes of the vibronic $\tilde{A}^2A_1$ states of H_2S^+," Chem. Phys. Lett. **36**(3), 353–356 (1975).

[23] A. D. Webb, R. N. Dixon, and M. N. R. Ashfold, "Imaging studies of the photodissociation of H_2S^+ cations. I. Illustrations of the role of nuclear spin," J. Chem. Phys. **127**(22), 224307 (2007).

[24] A. D. Webb, N. Kawanaka, R. N. Dixon, and M. N. R. Ashfold, "Imaging studies of the photodissociation of H_2S^+ cations. II," J. Chem. Phys. **127**(22), 224308 (2007).

[25] A. Skancke *et al.*, "An ab initio SCF-MO calculation of methylenecyclopropene, cyclopropenimine, and cyclopropenone," Acta Chem. Scand. **27**(9), 3243–3250 (1973).

[26] H. Sakai, S. Yamabe, T. Yamabe, K. Fukui, and H. Kato, "Ab initio MO calculations on the electronics structures of H_2S^+ and H_2O^+," Chem. Phys. Lett. **25**(4), 541–545 (1974).

[27] G. Hirsch and P. J. Bruna, "Ab initio MRD–CI study on H_2S^+. Dissociation correlation diagram for the $\tilde{A}\ ^2A_1$ and $\tilde{B}\ ^2B_2$ electronic states," Int. J. Mass Spectrom. Ion Phys. **36**(1), 37–46 (1980).

[28] I. Tokue, K. Yamasaki, and S. Nanbu, "$He^*(2^3S)$ penning ionization of H_2S. I. Theoretical Franck–Condon factors for the $H_2S(\tilde{X}\ ^1A_1, v'=0) \rightarrow H_2S^+(\tilde{X}\ ^2B_1, \tilde{A}\ ^2A_1)$ ionization and $H_2S^+(\tilde{A}–\tilde{X})$ transition," J. Chem. Phys. **119**(12), 5874–5881 (2003).

[29] W. Z. Li and M. B. Huang, "The $1^2A''$, $1^2A'$, and $2^2A'$ electronic states of the H_2S^+ ion studied using multiconfiguration second-order perturbation theory," Chem. Phys. **315**(1–2), 133–141 (2005).

[30] Z. Luan, Y. Fu, Y. Tan, Y. Wang, B. Shan, J. Li, X. Zhou, W. Chen, L. Liu, B. Fu, D. H. Zhang, X. Yang, and X. Wang, "Observation of competitive nonadiabatic photodissociation dynamics of H_2S^+ cations," J. Phys. Chem. Lett. **13**(34), 8157–8162 (2022).

[31] Z. Luan, Y. Fu, Y. Tan, Y. Wang, A. Liu, T. Wang, X. Zhou, B. Fu, D. H. Zhang, D. Yuan, X. Wang, and X. Yang, "Photodissociation dynamics of H_2S^+ near 325 nm," Chin. J. Chem. Phys. **36**(3), 289–297 (2023).
[32] J. Li, Y. L. Wang, Y. X. Tan, N. Zhang, W. X. Wang, L. R. Hu, D. F. Yuan, X. A. Wang, and X. M. Yang, "Photodissociation dynamics of H_2S^+ via A^2A_1 (1, 8, 0) excited state," Chin. J. Chem. Phys. **37**(2), 271–278 (2024).
[33] A. H. Zanganeh, J. H. Fillion, J. Ruiz, M. Castillejo, J. L. Lemaire, N. Shafizadeh, and F. Rostas, "Photodissociation of H_2O and D_2O below 132 nm," J. Chem. Phys. **112**(13), 5660–5671 (2000).
[34] J. H. Fillion, R. van Harrevelt, J. Ruiz, M. Castillejo, A. H. Zanganeh, J. L. Lemaire, M. C. van Hemert, and F. Rostas, "Photodissociation of H_2O and D_2O in $\tilde{B}$, $\tilde{C}$, and $\tilde{D}$ states (134–119 nm). Comparison between experiment and ab initio calculations," J. Phys. Chem. A **105**(51), 11414–11424 (2001).
[35] I. Hanazaki, "Fragment rotational excitation due to the parent rotation in the dissociation of molecules," Chem. Phys. Lett. **218**(1–2), 151–158 (1994).
[36] K. J. Yuan, Y. Cheng, L. Cheng, Q. Guo, D. X. Dai, X. Y. Wang, X. M. Yang, and R. N. Dixon, "Nonadiabatic dissociation dynamics in H_2O: Competition between rotationally and nonrotationally mediated pathways," Proc. Natl. Acad. Sci. U. S. A. **105**(49), 19148–19153 (2008).
[37] K. J. Yuan, Y. Cheng, L. N. Cheng, Q. Guo, D. X. Dai, X. M. Yang, and R. N. Dixon, "Quantum state-selected photodissociation dynamics of H_2O: Two-photon dissociation via the $\tilde{C}$ electronic state," J. Chem. Phys. **133**(13), 134301 (2010).
[38] Y. C. Wu, Z. X. Zhang, S. E. Zhang, Z. J. Luo, Y. R. Zhao, S. K. Yang, Z. X. Li, Y. Chang, Z. C. Chen, S. R. Yu, X. M. Yang, and K. J. Yuan, "Rotational state specific dissociation dynamics of D_2O via the $\tilde{C}$(010) state: The effect of bending vibrational excitation," J. Chem. Phys. **156**(21), 214301 (2022).
[39] S. H. Kable, J. C. Loison, D. W. Neyer, P. L. Houston, I. Burak, and R. N. Dixon, "Observation of a parallel recoil distribution from a perpendicular absorption transition in formyl radicals HCO and DCO," J. Phys. Chem. **95**(21), 8013–8018 (1991).
[40] X. X. Hu, L. S. Zhou, and D. Q. Xie, "State-to-state photodissociation dynamics of the water molecule," Wiley Interdiscip. Rev.: Comput. Mol. Sci. **8**(2), e1350 (2018).
[41] B. Jiang, D. Q. Xie, and H. Guo, "Communication: State-to-state differential cross sections for $H_2O(\tilde{B})$ photodissociation," J. Chem. Phys. **134**(23), 231103 (2011).
[42] Y. Cheng, K. J. Yuan, L. N. Cheng, Q. Guo, D. X. Dai, and X. M. Yang, "Photodissociation dynamics of H_2O: Effect of unstable resonances on the $\tilde{B}\,^1A_1$ electronic state," J. Chem. Phys. **134**(6), 064301 (2011).